Combust. Sci. and Tech., 177: 1109–1150, 2005

ISSN: 0010-2202 print/1563-521X online
DOI: 10.1080/00102200590927012

Taylor & Francis
Taylor & Francis Group

A GENERALIZED MODEL OF ACOUSTIC RESPONSE OF TURBULENT PREMIXED FLAME AND ITS APPLICATION TO GAS-TURBINE COMBUSTION INSTABILITY ANALYSIS

DANNING YOU
YING HUANG
VIGOR YANG*

Department of Mechanical and Nuclear Engineering, Pennsylvania State University, University Park, Pennsylvania, USA

An analytical model is developed to study the combustion response of turbulent premixed flames to acoustic oscillations. The analysis is based on a level-set flamelet model, and accommodates spatial variations in chamber geometry and mean-flow properties. All known factors affecting the flame response to local flow disturbances are analyzed. A triple decomposition technique, which expresses each flow variable as the sum of a long-time-averaged, a periodic, and a turbulent component, is used to examine the interactions between acoustic and turbulent motions and their collective influence on the flame dynamics. As specific examples, both a simple and an enveloped flame commonly observed in a swirl-stabilized combustor are studied. The resultant flame response is incorporated into a three-dimensional acoustic analysis to determine the stability

Received 26 February 2004; accepted 19 May 2004.

This paper is dedicated to Professor Forman Williams on the occasion of his 70th birthday. Professor Williams is widely known and appreciated for his enormous contributions to the combustion community. The authors are indebted to him in that our first knowledge about combustion originated from his masterpiece *Combustion Theory* published by Addison-Wesley Publishing Company in 1965. The research work reported in this paper was sponsored by the Air Force Office of Scientific Research, Grant No. F49620-99-1-0290.

*Address correspondence to vigor@psu.edu

characteristics of a model gas-turbine combustor. Results are consistent with experimental observations and numerical simulations in terms of the stability boundary and acoustic wave properties. In particular, the enveloped flame tends to be resonantly coupled with the acoustic velocity oscillation, leading to large excursions of combustion oscillations.

Keywords: combustion response, premixed turbulent flame, acoustic disturbance, combustion instability, flamelet model, triple decomposition

INTRODUCTION

Combustion instabilities represent one of the most serious problems in the development of lean premixed gas-turbine engines (Lieuwen and McManus, 2003). The coupling between flame and flow dynamics provides the major energy to drive unsteady motions in a combustor. Several acoustic analyses have been developed to study this phenomenon by solving the wave equation for the oscillatory field (Dowling and Stow, 2003; You, 2004). As part of the formulation, the response of heat release to acoustic disturbances must be established to represent the energy source of flow oscillations. A number of analytical models were developed to characterize such responses for premixed flames based on the flamelet assumption. Marble and Candel (1978) appear to have performed the first two-dimensional analysis of flame response to acoustic waves. The work was based on an integral formulation within which the conservation equations are integrated with respect to the vertical coordinate. The combustor was decomposed into a flow of reactants and a region of combustion products, separated by an infinitesimally thin flame sheet anchored by a point flame holder. The oscillatory flow properties in the unburnt and burnt regions were matched at the flame sheet by taking into account the kinematic and conservation relations to determine the system dynamics under the effects of longitudinal flow oscillations. Because the mean flow appears only in integrals, the consequent errors in its presentation tend to be softened. Results indicate that the flame acts as a damper for disturbances arising downstream. The trend, however, is reversed for disturbances arising upstream in a certain frequency range. The frequency spectrum of the acoustic reflection coefficient at the flame front can be expressed with a flame Strouhal number defined as $\omega L/S_u$, with ω being the radian frequency of oscillation, L the

flame length, and S_u the flame speed. The same approach was followed with similar studies by Subbaiah (1983) and Poinsot and Candel (1988). It was also extended by Yang and Culick (1986) to investigate the combustion instability in a ramjet engine with a coaxial dump combustor. Recently, Wang and Yang (1997) applied the integral method to characterize the flame response to longitudinal acoustic waves in a swirl-stabilized combustor in a study of gas-turbine combustion instabilities.

The aforementioned analyses, although accommodating the spatial evolution of the mean and oscillatory flow properties and providing reasonable comparison with experimental data, generally require the numerical solution of a set of ordinary differential equations governing the flow and flame dynamics. A closed-form solution for the harmonic excitation of the flame front, however, can be obtained if the density variation across the flame is ignored. This assumption amounts to a constant mean-flow velocity throughout the entire flame zone, and is valid only for mixtures with low equivalence ratios. Fleifil et al. (1996) examined a conical laminar flame stabilized by a ring in a cylindrical duct with a uniform distribution of acoustic velocity along the flame axis. The mean velocity is of the Poiseuille type. The flame dynamics are found to be governed by two parameters, a reduced frequency normalized by the flame speed and the duct radius, $\omega R/S_L$, and the ratio of the flame speed to the mean-flow velocity, $S_L/\overline{u}$. The flame behaves like a high-pass filter in the sense that high-frequency oscillations pass through the flame without significantly affecting the heat-release rate, although the flame surface becomes wrinkled when the reduced frequency exceeds a critical value. Low-frequency oscillations, on the other hand, exert a strong influence on the heat-release fluctuation. The transfer function between disturbances in heat-release rate and impressed velocity disturbance is unity in the limit of zero frequency, and decreases with increasing frequency.

The constant flame-speed approach of Fleifil et al. (1996) was later extended by Hubbard and Dowling (1998) and Dowling (1999) to model the unsteady behavior of a ducted flame stabilized by a centerbody. Turbulent flames were considered by simply replacing the laminar flame speed in the formulation with its turbulent counterpart. This analysis took account of the effect of mixture-composition variation, which dominates the overall flame response at fuel-lean conditions through the influence on the flame speed. Schuller et al. (2003) examined two different configurations of laminar flames, one anchored by the rim of a circular duct (i.e., conical flame) and the other by a central rod in a duct (i.e.,

V-shaped flame). In both situations there was a uniform distribution of velocity perturbation and an axial convective wave along the flame. The V-shaped flame was shown to act as an amplifier of the acoustic velocity in a certain range of frequencies, indicating that it is more susceptible to combustion instabilities than conical flames. The uniform-disturbance model is at the low-frequency limit of the convective-wave model, and cannot predict this amplification.

Lieuwen (2003) recently reviewed the interactions between acoustic waves and premixed combustion processes. Two transfer functions characterizing the laminar flame response to velocity and equivalence-ratio perturbations were examined. The former can be expressed as a time-lag model under low-frequency conditions, with the interaction index determined by the laminar flame speed and the time lag by the flame length and mean-flow velocity. The latter, however, cannot be governed by a time lag, due to the complex dependence of the flame speed and heat of reaction on equivalence ratio. Other issues such as distributed reaction models and nonlinear responses of flames to finite amplitude perturbations are also discussed.

Most previous studies only dealt with longitudinal disturbances along the major flow direction and employed many simplified treatments. In reality, three-dimensional oscillations are commonly observed in operational combustors (Hsiao et al., 1998; Huang et al., 2003). The present work attempts to improve the predictive capabilities of existing models by developing a unified framework that allows for a systematic treatment of combustion instabilities in gas-turbine engines with lean premixed combustion. The approach starts with the modeling of turbulent flame dynamics in an acoustic environment. The analysis is based on an extended flamelet approach and accommodates spatial variations of chamber geometries and mean-flow properties. All known factors affecting the flame response to local flow disturbances are analyzed. The resultant combustion response functions are then formulated in such a manner that they can be effectively incorporated into a generalized acoustic instability analysis. Unlike most currently available models, this one is capable of handling situations with complicated flow fields under various distributed and surface effects. Both longitudinal and transverse oscillations are treated over a broad range of frequencies.

The paper is structured as follows. In Section 2, a generalized analysis of the acoustic response of a premixed turbulent flame to impressed flow oscillations is developed. Various attributes dictating the flame

dynamics are formulated and analyzed. Section 3 deals with the formulation of combustion response functions. Section 4 briefly describes a three-dimensional acoustic analysis for predicting combustion instabilities in complex geometries with nonuniform mean flow fields. Finally, as a specific example, the oscillatory field in a swirl-stabilized combustor is examined.

FLAME RESPONSE TO ACOUSTIC EXCITATION

Flame Surface Displacement

Most previous works on flame response to acoustic excitations have focused on laminar conditions. Very limited attention was given to turbulent flames, except for some rudimentary treatments that simply replace the laminar flame speed with its turbulent counterpart. Unlike laminar cases, however, turbulent combustion involves an array of intricate physiochemical processes with wide disparities of length and time scales. The turbulence/chemistry interactions in premixed flames can be characterized by several nondimensional parameters: turbulent Reynolds number $\mathrm{Re} \approx v' l / S_L l_F$, turbulent Damköhler number $Da \approx S_L l / v' l_F$, and turbulent Karlovitz number $Ka \approx l_F^2 / \eta^2$ (Williams, 1985; Peters, 2000). The variable v' denotes the turbulent velocity fluctuation, l the integral length scale of turbulence, S_L and l_F the laminar flame speed and thickness, respectively, and η the Kolmogorov length scale. An additional Karlovitz number, Ka_δ, defined as the square of the ratio of the flame inner layer thickness l_δ to the Kolmogorov length scale η, is also introduced. Based on the relative magnitudes of these parameters, premixed turbulent combustion can be classified into four different regimes: broken reaction zone ($\mathrm{Re} > 1,\ v'/S_L > 1$ and $Ka_\delta > 1$), thin reaction zone ($\mathrm{Re} > 1,\ v'/S_L > 1,\ Ka > 1$ and $Ka_\delta < 1$), corrugated flamelets ($\mathrm{Re} > 1,\ v'/S_L > 1$ and $Ka < 1,\ Da > 1$), and wrinkled flamelet regime ($\mathrm{Re} > 1$, $\mathrm{Re} > 1,\ v'/S_L < 1, Ka < 1$ and $Da > 1$) (Peters, 2000). In both the thin reaction-zone and flamelet regimes, the inner layer of the laminar flame structure is not affected by turbulence. The premixed turbulent flame can be treated as a synthesis of thin reaction-diffusion layers, commonly referred to as flamelets, embedded in an otherwise inert turbulent flow field. Although combustion may occur in the broken reaction-zone regime in certain circumstances, such as the lean blowout phenomenon in a gas-turbine combustor (Eggenspieler and Menon, 2004), chemical reactions are often confined in thin, sheetlike flamelets under most

conditions in many practical combustion devices (Poinsot et al., 1991; Liñán and Williams, 1993; Peters, 2000). The situation holds especially true for the study of flame dynamics in a lean premixed gas-turbine combustor (Huang et al., 2003). Thus, the flamelet description is employed in the current work, which treats the complicated chemistry problem separately from the flow analysis. The flame propagates locally with the laminar flame speed and the effect of turbulence is to wrinkle the flame and subsequently increase its surface area.

To evaluate the flame response to an acoustic velocity perturbation, an analytic model is derived. Under the flamelet assumption, the flame movement can be tracked using a field variable G and the location of the flame front is assigned to a particular level $G = G_0$. The flame surface propagates in the normal direction at a speed S_L relative to the unburnt mixture with the local velocity $\boldsymbol{u}$. The evolution of the flame surface can be described using the following transport equation, commonly known as the G-equation (Williams, 1985; Kerstein et al., 1988):

$$\frac{\partial G}{\partial t} + \boldsymbol{u} \cdot \nabla G - S_L |\nabla G| = 0 \tag{1}$$

Both random and periodic (coherent) motions exist in many practical turbulent flows. The intricate coupling between these flow motions and flame plays an important role in determining the characteristics of turbulent combustion. The effects of coherent structures on the propagation of premixed flames were investigated by Ulitsky and Collins (1997). Their results indicate that the turbulent burning rate is enhanced by coherent structures. Lieuwen (2002) analyzed acoustic wave interactions with turbulent premixed flames, and found that with increased flame wrinkling, the coherent field becomes increasingly independent of the temperature jump across the flame and response of the mass-burning rate. In addition, the flame wrinkling acts as a damper of acoustic energy. A triple decomposition technique, which allows the random and periodic motions to be separated from each other, was previously developed to study coherent structures in turbulent shear flows (Hussain and Reynolds, 1970; Liu, 1989). This method was extended by Apte and Yang (2002) to study the interactions between acoustic waves and turbulent flow motions. In the present work, the triple decomposition technique is employed to investigate the effects of acoustic oscillations and turbulence on the periodic behavior of a turbulent flame. Following the approach of Apte and Yang (2002), each flow variable is expressed as

the sum of a long-time-averaged, a periodic (coherent), and a turbulent (stochastic) quantity as follows.

$$\Im(\boldsymbol{r},t)=\overline{\Im}(\boldsymbol{r})+\Im'(\boldsymbol{r},t)=\overline{\Im}(\boldsymbol{r})+\Im^a(\boldsymbol{r},t)+\Im^t(\boldsymbol{r},t) \tag{2}$$

The decomposition can be achieved using the long-time- and ensemble-averaging operations defined below.

long- time averaging

$$\overline{\Im}(\boldsymbol{x})=\left(\lim_{N\to\infty}\frac{1}{N}\sum_{n=0}^{N-1}\Im(\boldsymbol{x},t_0+n\Delta t)\right),\ \text{where } N\Delta t\gg\tau\gg\Delta t \tag{3}$$

ensemble averaging

$$\langle\Im(\boldsymbol{x},t)\rangle=\lim_{N\to\infty}\frac{1}{N}\sum_{n=0}^{N-1}\Im(\boldsymbol{x},t+n\tau) \tag{4}$$

so that

$$\langle\Im(\boldsymbol{x},t)\rangle=\overline{\Im}(\boldsymbol{x})+\Im^a(\boldsymbol{x},t) \tag{5}$$

where τ is the period of acoustic oscillation and t_0 is the temporal location at which steady periodic motions are obtained.

Applying the time-averaging operation to Eq. (1), we obtain the equation for $\overline{G}$

$$\overline{\boldsymbol{u}}\cdot\nabla\overline{G}+\overline{\boldsymbol{u}^a\cdot\nabla G^a}=\overline{S_L|\nabla G|}-\overline{\boldsymbol{u}^t\cdot\nabla G^t} \tag{6}$$

The equation for G^a can be obtained by taking the ensemble average of Eq. (1) and subtracting Eq. (6) from the result.

$$\frac{\partial G^a}{\partial t}+\boldsymbol{u}\cdot\nabla G^a+\boldsymbol{u}^a\cdot\nabla\overline{G}+\boldsymbol{u}^a\cdot\nabla G^a-\overline{\boldsymbol{u}^a\cdot\nabla G^a}=(S_L|\nabla G|)^a-(\boldsymbol{u}^t\cdot\nabla G^t)^a \tag{7}$$

Both Eqs. (6) and (7) have two unclosed terms on the right-hand side, which need to be modeled either analytically or empirically. The term $\overline{S_L|\nabla G|}$ represents the propagation of the long-time-averaged flame front, and the term $(S_L|\nabla G|)^a=\langle S_L|\nabla G|\rangle-\overline{S_L|\nabla G|}$ is related to the propagation of the periodic oscillation of the flame surface. They can be modeled through the introduction of a turbulent flame speed $\overline{S}_T$.

$$\overline{S_L|\nabla G|}=\overline{S}_T\left|\nabla\overline{G}\right|=\overline{S}_T(-\bar{\boldsymbol{n}}\cdot\nabla\overline{G}) \tag{8}$$

$$(S_L|\nabla G|)^a=\overline{S}_T(-\bar{\boldsymbol{n}}\cdot\nabla G^a) \tag{9}$$

where $\bar{\boldsymbol{n}}=-\nabla\overline{G}/|\nabla\overline{G}|$. The periodic flame surface is assumed to propagate with the same speed in the normal direction $\bar{\boldsymbol{n}}$ as for the mean quantity, an approximation strictly valid for small amplitude oscillations.

The terms $\overline{\boldsymbol{u}^t\cdot\nabla G^t}$ and $(\boldsymbol{u}^t\cdot\nabla G^t)^a$ are associated with turbulence transport. Because the original G-equation is parabolic, they cannot be approximated using the classical gradient-transport approach, which leads to the reduction to an elliptic equation. According to Peters (2000), the gradient flux approximation is split into a normal diffusion and a curvature term. The former is already included in the flame speed model and needs to be removed. Therefore, only the curvature term is retained.

$$\overline{\boldsymbol{u}^t\cdot\nabla G^t}=-\nu_t\bar{k}|\nabla\overline{G}|=-\nu_t\bar{k}\cdot\bar{\boldsymbol{n}}\cdot\nabla\overline{G} \tag{10}$$

$$(\boldsymbol{u}^t\cdot\nabla G^t)^a=-\nu_t\bar{k}\cdot\bar{\boldsymbol{n}}\cdot\nabla G^a \tag{11}$$

where ν_t is the turbulent eddy viscosity, which is proportional to the product of the characteristic turbulent length and velocity scales. $\bar{k}$ is the mean flame front curvature, $\bar{k}=\nabla\cdot\bar{\boldsymbol{n}}$. Substitution of Eqs. (8)–(11) into Eqs. (6) and (7) leads to the modeled equations for $\overline{G}$ and G^a.

$$\bar{\boldsymbol{u}}\cdot\nabla\overline{G}+\overline{\boldsymbol{u}^a\cdot\nabla G^a}=(\overline{S}_T+\nu_t\bar{k})\cdot\frac{\nabla\overline{G}}{|\nabla\overline{G}|}\cdot\nabla\overline{G} \tag{12}$$

$$\frac{\partial G^a}{\partial t}+\bar{\boldsymbol{u}}\cdot\nabla G^a+\boldsymbol{u}^a\cdot\nabla\overline{G}+\boldsymbol{u}^a\cdot\nabla G^a-\overline{\boldsymbol{u}^a\cdot\nabla G^a}=(\overline{S}_T+\nu_t\bar{k})\cdot\frac{\nabla\overline{G}}{|\nabla\overline{G}|}\cdot\nabla G^a \tag{13}$$

A more detailed description of the modeling approach has been given by Huang (2003).

To facilitate formulation of the flame response, we consider an axisymmetric configuration shown schematically in Figure 1. Lean premixed combustible gases are delivered to a dump chamber, and the flame is stabilized in the wake of the centerbody (Huang et al., 2003; Huang and Yang, 2004). The variable G is expressed as

$$G(x,r,t)=x-\xi(r,t) \tag{14}$$

where $\xi(r,t)$ is the instantaneous axial displacement of the flame front. The above equation is valid only when $\xi(r,t)$ is a single-valued function of r. Accordingly, the time-averaged and periodical flame surfaces can be

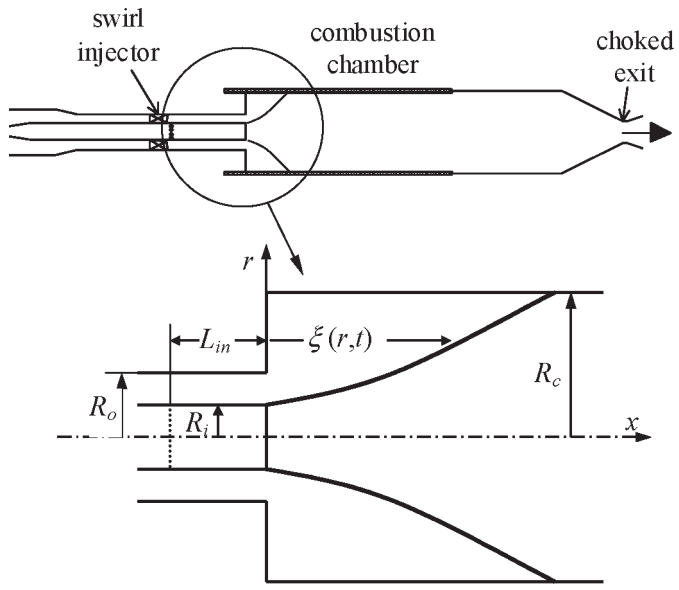

Figure 1. Schematic of a swirl-stabilized model gas-turbine combustor.

expressed as

$$\overline{G}(x,r,t) = x - \bar{\xi}(r) \text{ and } G^a(x,r,t) = -\xi^a(r,t) \tag{15}$$

Substitution of Eq. (15) into Eqs. (12) and (13) and rearrangement of the results leads to the equations for the mean and periodically fluctuating components of the flame-surface displacement in a cylindrical coordinate system. Both the nonlinear terms and the curvature terms are neglected to simplify the analysis.

$$\bar{u} - \bar{v} \cdot d\bar{\xi}/dr - \overline{S}_T \left[\left(d\bar{\xi}/dr \right)^2 + 1 \right]^{1/2} = 0 \tag{16}$$

$$\frac{\partial \xi^a}{\partial t} + \left\{ \bar{v} + \overline{S}_T \left[\left(\frac{d\bar{\xi}}{dr} \right)^2 + 1 \right]^{-1/2} \frac{d\bar{\xi}}{dr} \right\} \frac{\partial \xi^a}{\partial r} = \left(u^a - v^a \frac{d\bar{\xi}}{dr} \right) \tag{17}$$

The mean velocity components, $\bar{u}$ and $\bar{v}$, and flame displacement $\bar{\xi}(r)$ can be determined from a separate numerical analysis, which solves the

complete conservation equations (e.g., Wang and Yang, 1997; Huang et al., 2003). The turbulent flame speed $\overline{S}_T$ can be deduced directly from Eq. (16).

$$\overline{S}_T = \left(\bar{u} - \bar{v}\cdot d\bar{\xi}/dr\right) \Big/ \left[\left(d\bar{\xi}/dr\right)^2 + 1\right]^{1/2} \tag{18}$$

For linear perturbations with a radian frequency Ω, the time-harmonic and the spatial-dependent parts of each flow variable are separated.

$$\begin{aligned} u^a(\boldsymbol{r}, t) &= \hat{\boldsymbol{u}}(\boldsymbol{r}) \exp(i\Omega t) \\ v^a(\boldsymbol{r}, t) &= \hat{v}(\boldsymbol{r}) \exp(i\Omega t) \\ \xi^a(\boldsymbol{r}, t) &= \hat{\xi}(\boldsymbol{r}) \exp(i\Omega t) \end{aligned} \tag{19}$$

Substitution of Eq. (19) into Eq. (17) gives a first-order ordinary differential equation for the periodic oscillation of the flame displacement

$$\left\{\bar{v} + \overline{S}_T\left[\left(d\bar{\xi}/dr\right)^2 + 1\right]^{-1/2} \cdot d\bar{\xi}/dr\right\}\frac{d\hat{\xi}}{dr} + i\Omega\hat{\xi} - \left(\hat{u} - \hat{v}\cdot d\bar{\xi}/dr\right) = 0 \tag{20}$$

Owing to the spatial variation of the mean flow and the acoustic disturbances, the above equation usually requires numerical integration, subject to proper boundary conditions. An analytical solution, however, exists if the flame spreading angle and flow velocity remain fixed in the region of concern. We may take advantage of this and discretize the flame in small sections, such that the mean-flow properties are uniformly distributed in each section, as shown schematically in Figure 2. By applying the boundary conditions that $\bar{\xi}(R_i) = \xi^a(R_i, t) = 0$, the

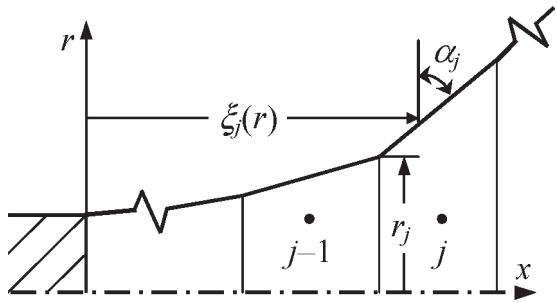

Figure 2. Piecewise treatment of flame zone.

time-averaged flame displacement becomes a piecewise function

$$\begin{aligned}\bar{\xi}_1(r) &= (r - R_i)\tan\alpha_1, \quad \text{for } r_1 \le r \le r_2 \\ \bar{\xi}_j(r) &= \left(r - r_j\right)\tan\alpha_j + \sum_{k=2}^{j}\left[(r_k - r_{k-1})\tan\alpha_k\right], \quad \text{for } r_j \le r \le r_{j+1}\end{aligned} \tag{21}$$

where j denotes the section number, r_j the radial coordinate of the flame front at the intersection point between sections j and j–1, and α_j the flame angle in section j. Note that $r_1 = R_i$. We substitute Eq. (21) into Eq. (20) and solve for the periodical fluctuation of the flame displacement.

$$\begin{aligned}\hat{\xi}_1(r) &= \frac{\hat{u}_{n,1}}{i\Omega}\left[1 - \exp\left(\frac{-i\Omega(r - R_1)}{\overline{U}_{\alpha,1}}\right)\right], \quad \text{for } r_1 \le r \le r_2 \\ \hat{\xi}_j(r) &= \frac{\hat{u}_{n,j}}{i\Omega}\left[1 - \exp\left(\frac{-i\Omega\left(r - r_j\right)}{\overline{U}_{\alpha,j}}\right)\right] \\ &\quad + \hat{\xi}_{j-1}(r_j)\exp\left(\frac{-i\Omega\left(r - r_j\right)}{\overline{U}_{\alpha,j}}\right), \quad \text{for } r_j \le r \le r_{j+1}\end{aligned} \tag{22}$$

where $\overline{U}_{\alpha,j} = \bar{v}_j + \overline{S}_{T,j}\sin\alpha_j$, and $\hat{u}_{n,j} = \hat{u}_j - \hat{v}_j\tan\alpha_j$.

Within the flamelet formulation, the rate of heat release is directly proportional to the flame surface area. Its specific quantity at the ensemble-averaged flame location can be readily obtained from

$$A_{\langle\xi_j\rangle} = \frac{1}{\Delta x}\left[\left(\partial\langle\xi_j\rangle/\partial r\right)^2 + 1\right]^{1/2} \tag{23}$$

where Δx denotes the unit axial length. $\langle\xi\rangle = \bar{\xi} + \xi^a$ represents the ensemble-averaged flame location. $A_{\langle\xi\rangle}$ can be further expressed as $A_{\langle\xi\rangle} = A_{\bar{\xi}} + A_{\xi^a}$, where $A_{\bar{\xi}}$ is the specific surface area at the long-time-averaged flame location, and A_{ξ}^{a} the area increase due to the periodic flame displacement.

Response to Uniformly Distributed Disturbance

To provide direct insight into the flame dynamics in an acoustic environment, we consider a simple configuration, as shown schematically in Figure 3*a*. The mean-flow velocity is assumed to be uniform, and the flame spreading angle is constant. This limiting case amounts to the neglect of the density variation across the flame, an approximation only valid for mixtures with extremely low equivalence ratios. Under this

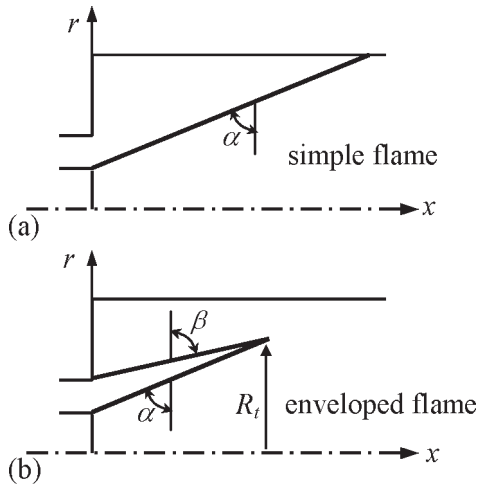

Figure 3. (*a*) Simple flame anchored at centerbody; (*b*) enveloped flame anchored at centerbody and rear-facing step.

condition, the fluctuating flame displacement can be derived as

$$\frac{\xi^a}{R_c - R_i} = \frac{1}{i\Omega_u}\left[\frac{u^a}{\bar{u}} + \frac{v^a}{\bar{v}}C_r\right]\left[1 - \exp\left(-i\Omega_f \frac{r - R_i}{R_c - R_i}\right)\right] \tag{24}$$

The normalized fluctuation of the flame displacement depends on three parameters: Ω_f, Ω_u, and C_r. The coefficient C_r is defined as $C_r = \overline{S}_T/(\bar{u}\cos\alpha) - 1$, where the first term is the ratio of the turbulent flame speed to the projection of the axial mean-flow velocity in the direction normal to the flame front. Since a flame remains at a fixed location if the approaching flow velocity of the unburnt mixture normal to the flame surface is equal to the flame speed, the value of C_r represents a degree of flame flashback. The flame Strouhal number, Ω_f, is associated with the flame speed in the radial direction.

$$\Omega_f = \Omega(R_c - R_i)/\left(\bar{v} + \overline{S}_T \sin\alpha\right) \tag{25}$$

The flow Strouhal number, Ω_u, is defined based on the mean axial velocity.

$$\Omega_u = \Omega(R_c - R_i)/\bar{u} \tag{26}$$

Therefore, the flow Strouhal number and C_r determine the amplitude of the flame surface oscillation, and the flame Strouhal number defines its

spatial distribution. It can be predicted from Eq. (24) that when Ω_f increases, the flame surface becomes more wrinkled, and when Ω_u increases, the oscillation amplitude decreases. The same phenomena were observed by Fleifil et al. (1996).

A simple manipulation of Eq. (24) indicates that there exists a wave structure on the disturbed flame surface. The corresponding wavelength λ and wave envelope are given respectively by

$$\lambda = 2\pi(R_c - R_i)/\Omega_f$$
$$\left|\frac{\xi^a}{R_c - R_i}\right| = \frac{2}{\Omega_u}\left[\frac{\hat{u}}{\bar{u}} + \frac{\hat{v}}{\bar{v}}C_r\right]\sin\left(\frac{\Omega_f}{2}\frac{r - R_i}{R_c - R_i}\right) \tag{27}$$

For a fixed flame-spreading angle, the flow Strouhal number can be calculated from the other two parameters.

$$\Omega_u = \Omega_f\left(\sin^2\alpha - C_r\cos^2\alpha\right)/\tan\alpha \tag{28}$$

Figures 4–6 show the temporal evolution of the instantaneous flame displacement within one cycle of oscillation for excitation frequencies of 100, 1000, and 10,000 Hz, respectively. The mean-flow properties

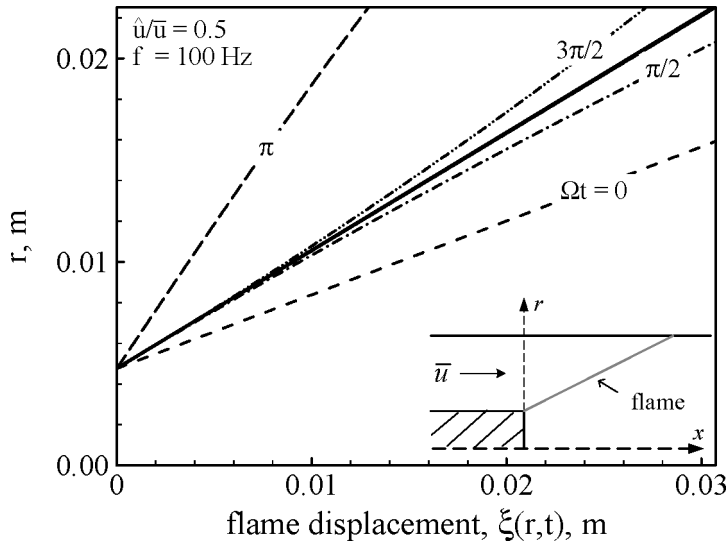

Figure 4. Temporal evolution of flame displacement within one cycle of oscillation, $\hat{u}/\bar{u} = 0.5$, $\hat{v}/\bar{v} = 0$, $\overline{S}_T/\bar{u} = 0.3$, $\alpha = 60^\circ$, and $f = 100$ Hz. Thick black line represents the mean flame location.

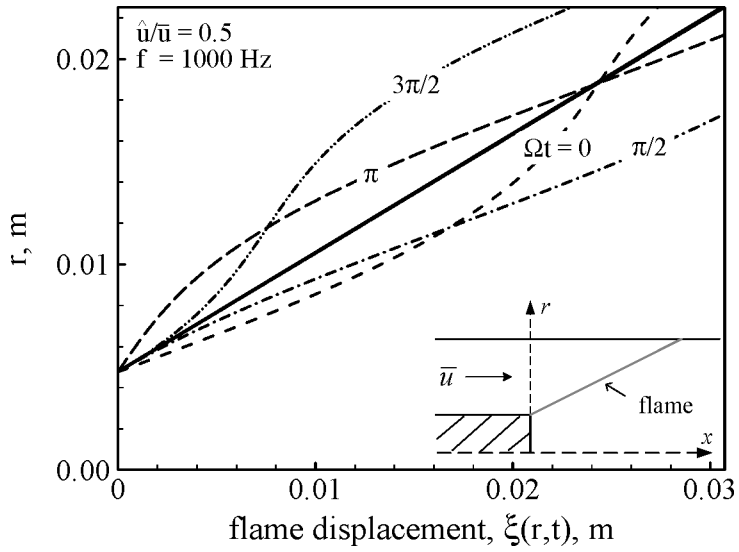

Figure 5. Temporal evolution of flame displacement within one cycle of oscillation, $\hat{u}/\bar{u} = 0.5$, $\hat{v}/\bar{v} = 0$, $\overline{S}_T/\bar{u} = 0.3$, $\alpha = 60^\circ$, and $f = 1000$ Hz. Thick black line represents the mean flame location.

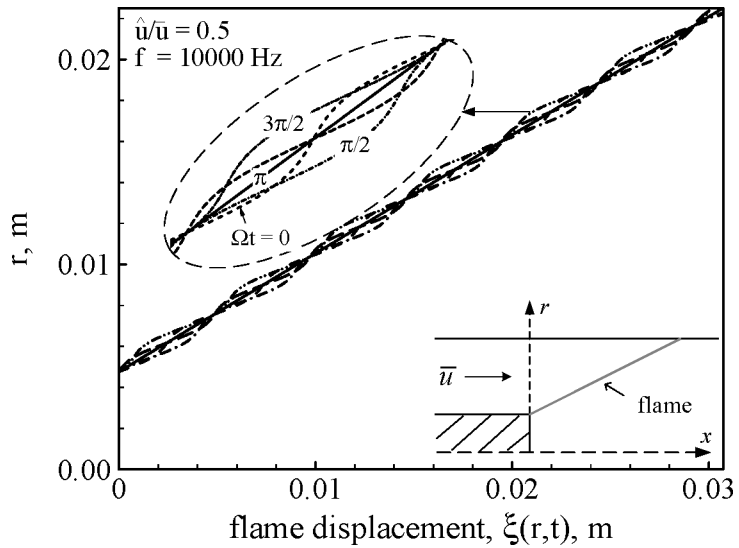

Figure 6. Temporal evolution of flame displacement within one cycle of oscillation, $\hat{u}/\bar{u} = 0.5$, $\hat{v}/\bar{v} = 0$, $\overline{S}_T/\bar{u} = 0.3$, $\alpha = 60^\circ$, and $f = 10,000$ Hz. Thick black line represents the mean flame location.

include $\alpha = 60^\circ$ and $\overline{S}_T/\bar{u} = 0.3$, and the acoustic velocity amplitudes are $\hat{u}/\bar{u} = 0.5$ and $\hat{v}/\bar{v} = 0$. At low frequencies of $f = 100$ and 1000 Hz, the surface wavelengths calculated by Eq. (27) are 0.28 and 0.028 m, respectively. They are thus greater than the characteristic flame scale $R_c - R_i$. The flame deviates from its mean location monotonically without obvious wavy structure, as evidenced in Figures 4 and 5. The situation, however, becomes drastically different at the high frequency $f = 10{,}000$ Hz. The flame exhibits periodic oscillations on its surface, and is more wrinkled with increasing frequency.

The total flame surface area is obtained by integrating the displacement over the flame surface.

$$A^g_{\langle\xi\rangle} = \int_{R_i}^{R_c} \left\{ 2\pi r \left[\left(\partial\langle\xi\rangle/\partial r \right)^2 + 1 \right]^{1/2} \right\} dr \tag{29}$$

where the superscript g denotes integration over the entire flame. After substitution of Eq. (24) into the above equation and some straightforward algebraic manipulations, we obtain the fluctuation of the total flame surface area normalized by its quantity at the time-mean position.

$$\frac{A^g_{\xi a}}{A^g_{\bar{\xi}}} = \left[\frac{2}{\left(R_c^2 - R_i^2 \right)} \int_{R_i}^{R_c} (r \cdot f) dr \right] - 1 \tag{30}$$

where

$$f = \left[1 + \frac{2u_n^a \tan\alpha \cos^2\alpha}{\overline{U}_\alpha} e^{\frac{-i\Omega(r-R_i)}{\overline{U}_\alpha}} + \left(\frac{\cos\alpha u_n^a}{\overline{U}_\alpha} \right)^2 e^{\frac{-2i\Omega(r-R_i)}{\overline{U}_\alpha}} \right]^{1/2} \tag{31}$$

Equation (30) can be numerically integrated to obtain the overall flame response to acoustic disturbances, defined by

$$\left(R^g_u \right)_u = \frac{A^g_{\xi a}/A^g_{\bar{\xi}}}{u^a/\bar{u}}, \quad \left(R^g_v \right)_u = \frac{A^g_{\xi a}/A^g_{\bar{\xi}}}{v^a/\bar{v}} \tag{32}$$

where the subscript u denotes the velocity sensitivity of the response function.

The above transfer functions between the disturbances in the overall flame surface area and flow velocity depend intimately on the flame Strouhal number Ω_f. Figure 7 shows the results for three different excitation amplitudes. The transfer function has a magnitude of unity at zero frequency, and decays sinusoidally with increasing frequency. The flame

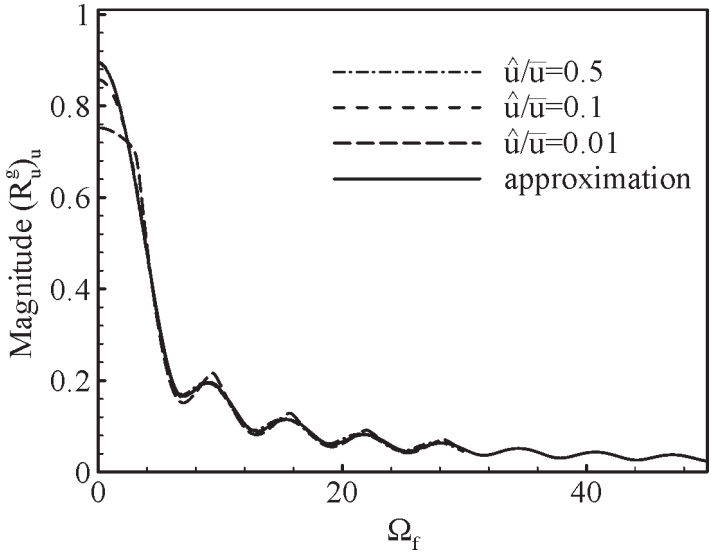

Figure 7. Magnitude of transfer function between fluctuations of overall flame surface area and flow velocity as function of flame Strouhal number $\Omega_f(\hat{v}/\bar{v}=0,\ \overline{S}_T/\bar{u}=0.3, \alpha=60^\circ)$.

undergoes a large excursion of oscillation at a low frequency, although its surface is less wrinkled. Similar observations were previously made by Fleifil et al. (1996) and Schuller et al. (2003). The magnitude of velocity fluctuation $\hat{u}/\bar{u}$ exerts little influence on the flame response, except in the low-frequency range.

Analytical solutions of the global flame response can be obtained for small disturbances. Applying the Taylor series expansion to Eq. (29) and neglecting higher-order terms, we obtain

$$A^g_{\xi^a} = \int_{R_i}^{R_c} \left[2\pi r\left[\left(d\bar{\xi}/dr\right)^2+1\right]^{-1/2} \frac{d\bar{\xi}}{dr}\frac{\partial \xi^a}{\partial r}\right] dr \tag{33}$$

The transfer function defined by Eq. (32) becomes

$$\left(R^g_u\right)_u = \frac{2(R_c-R_i)}{R_c+R_i}\frac{\bar{u}\sin\alpha\cos\alpha}{\Omega_f^2\overline{U}_\alpha}\left[\left(\frac{i\Omega_f R_c}{R_c-R_i}+1\right)\left(1-e^{-i\Omega_f}\right)-i\Omega_f\right] \tag{34}$$

The approximate amplitudes and phases of the global flame response $\left(R^g_u\right)_u$ calculated from Eq. (34) are compared with the numerical integration in Figure 7. It is shown that the perturbation amplitude has little effect on the approximate results. Good agreement between the analytical

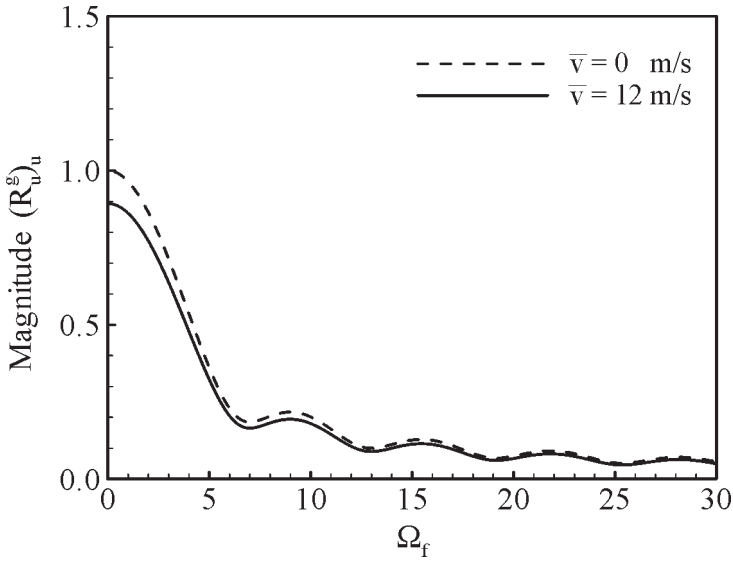

Figure 8. Magnitude of transfer function between fluctuations of overall flame surface area and flow velocity as function of flame Strouhal number $\Omega_f (\hat{v}/\bar{v} = 0,\ \overline{S}_T/\bar{u} = 0.3, \alpha = 60^\circ)$.

and numerical results is obtained. Thus, Eq. (34) serves as a reasonable approximation regardless of the oscillation amplitude.

If the mean-flow velocity in the radial direction is negligible compared to that in the axial direction, the transfer function given in Eq. (34) is identical to the result of the corresponding case studied by Schuller et al. (2003). Figure 8 compares the magnitude of $\left(R_u^g\right)_u$ under conditions with and without radial velocity $\bar{v}$. The finite radial velocity modifies the solution in the low-frequency region. The error is around 10% at zero frequency and decreases to below 2% for a flame Strouhal number greater than 5, corresponding to $f = 1260$ Hz in the sample problem. The acoustic oscillation frequencies of the specific case solved in Section 4 are all beyond this value. Thus, the effect of radial velocity can be neglected in most practical situations to simplify the combustion stability analysis.

Response to Nonuniformly Distributed Disturbance

To explore the effect of the spatial distribution of acoustic disturbance on the local flame response, Eq. (20) was integrated numerically to obtain the periodical fluctuation of flame displacement. Two sample

studies were conducted, with the same mean-flow conditions as in the previous limiting cases. In the first case, the oscillation frequency was selected to be 1000 Hz, such that only longitudinal acoustic motion exists in the combustion chamber. The disturbance takes the form

$$u^a = \hat{u}(r)e^{i\Omega t} = \tilde{u}e^{ik_x\bar{\xi}}e^{i\Omega t} \tag{35}$$

where $\tilde{u}$ represents the oscillation amplitude, and the axial wave number k_x is defined as

$$k_x = \Omega/\bar{a} = \Omega M/\bar{u} \tag{36}$$

Case 2 deals with the disturbance at a much higher frequency of 21970 Hz, whose wavelength corresponds to the axial length of the flame. At this frequency, the first radial mode is cut on, so that the disturbance becomes

$$u^a = \hat{u}(r)e^{i\Omega t} = \tilde{u}e^{i\Omega t}e^{ik_x\bar{\xi}}J_0(k_r r) \tag{37}$$

where J_0 is the zeroth-order Bessel function of the first kind, and the wave number k_r for the first radial mode is

$$k_r = 3.83/R_c \tag{38}$$

The axial wave number can be determined by

$$k_x^2 = (\Omega/\bar{a})^2 - k_r^2 \tag{39}$$

Figures 9 and 10 show the flame displacements under both uniform, $u^a = \hat{u}e^{i\Omega t} = \tilde{u}e^{i\Omega t}$, and nonuniform disturbances specified by Eqs. (35) and (37), for these two frequencies. The general behavior of these cases is similar. The flame, however, is more responsive to nonuniform disturbances and exhibits a higher-amplitude oscillation. Figure 11 shows the frequency spectrum of the magnitude of the flame response function. The effect of the spatial distribution of the impressed disturbance on the flame response is clearly observed.

COMBUSTION RESPONSE OF PREMIXED TURBULENT FLAME

Within the flamelet assumption, the rate of heat release per unit volume can be given by the following expression:

$$\dot{Q} = q\rho S_L A \tag{40}$$

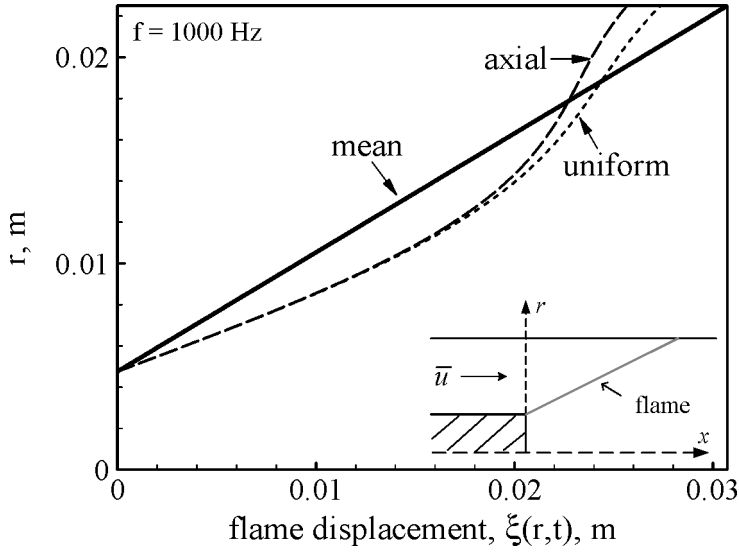

Figure 9. Flame displacement under uniform ($u^a = \tilde{u}e^{i\Omega t}$) and axial [Eq. (35)] disturbances, $\Omega t = 0, \tilde{u}/\bar{u} = 0.5, \hat{v}/\bar{v} = 0, \overline{S}_T/\bar{u} = 0.3, \bar{a} = 675\,\text{m/s}, \alpha = 60^\circ, M = 0.086,$ and $f = 1000\,\text{Hz}$. Thick black line represents the mean flame location.

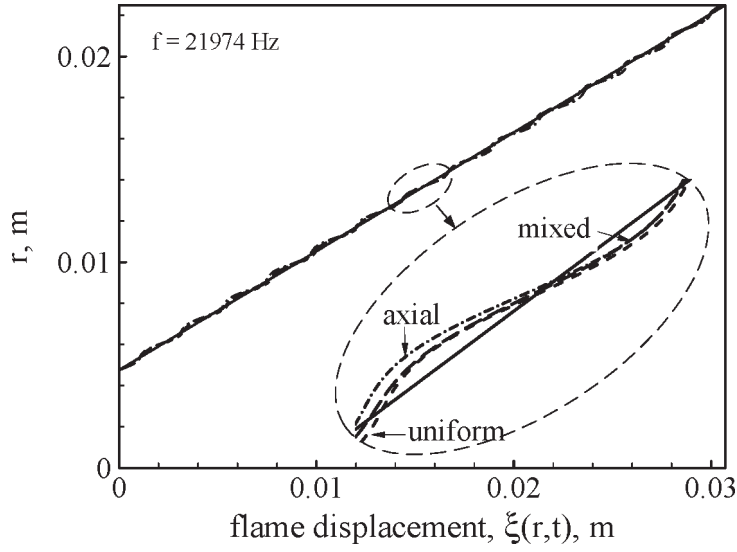

Figure 10. Flame displacement under uniform ($u^a = \tilde{u}e^{i\Omega t}$), axial [Eq. (35)], and mixed axial/radial [Eq. (37)] disturbances, $\Omega t = 0,\ \tilde{u}/\bar{u} = 0.5,\ \hat{v}/\bar{v} = 0,\ \overline{S}_T/\bar{u} = 0.3,\ \bar{a} = 675\,\text{m/s}, \alpha = 60^\circ, M = 0.086,$ and $f = 21974\,\text{Hz}$. Thick black line represents the mean flame location.

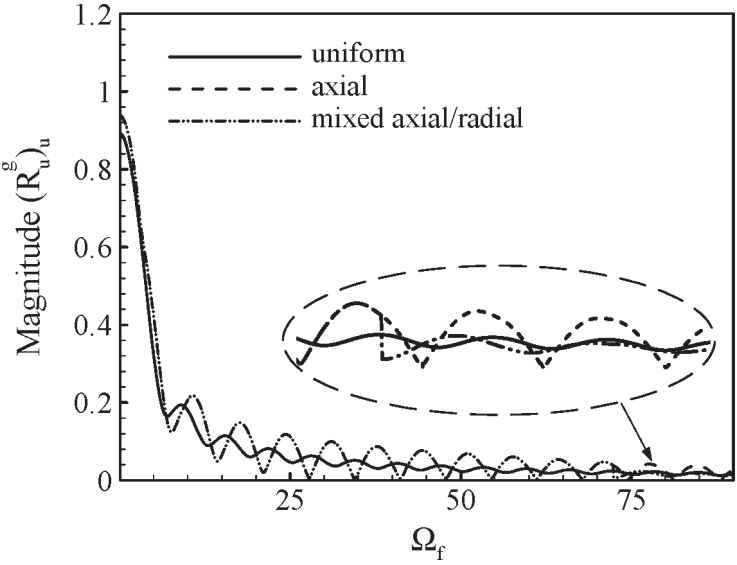

Figure 11. Effect of spatial variation of disturbance on transfer function between fluctuations of overall flame surface area and flow velocity as function of flame Strouhal number Ωf $(\tilde{u}/\bar{u} = 0.5,\ \hat{v}/\bar{v} = 0,\ \overline{S}_T/\bar{u} = 0.3,\ \bar{a} = 675\,\mathrm{m/s},\ \alpha = 60^\circ,\ M = 0.086)$.

where q is the heat of reaction per unit mass of reactants, ρ the unburnt mixture density, S_L the laminar flame speed, and A the specific flame-surface area. When the ensemble-averaging operation defined in Eqs. (3) and (4) is applied to Eq. (40), and only linear terms are retained, we obtain

$$\langle \dot{Q} \rangle = \langle \rho \rangle \langle q \rangle \langle S_L A \rangle \tag{41}$$

Unlike the long-time-averaged or ensemble-averaged flame locations and their associated surface areas, the instantaneous flame location and its corresponding surface area are very difficult to measure. To close the formulation, a turbulent flame speed, S_T, is introduced by enforcing the overall mass balance

$$S_T A_{\langle \xi \rangle} = \langle S_L A \rangle \tag{42}$$

Note that $A_{\langle \xi \rangle}$ differs from the ensemble-averaged flame-surface area $\langle A \rangle$, and the former is larger than the latter. Substitute the definition of turbulent flame speed S_T into Eq. (41) to obtain

$$\langle \dot{Q} \rangle = \langle \rho \rangle \langle q \rangle S_T A_{\langle \xi \rangle} \tag{43}$$

We now define the rate of heat release under a steady-state condition as

$$\overline{\dot{Q}} = \bar{q}\bar{\rho}\overline{S}_T A_{\bar{\xi}} \tag{44}$$

Subtracting Eq. (44) from Eq. (43), and neglecting higher-order terms, we have

$$\dot{Q}^a = q^a \bar{\rho}\overline{S}_T A_{\bar{\xi}} + \rho^a \overline{S}_T A_{\bar{\xi}}\bar{q} + \bar{\rho} S_T^a A_{\bar{\xi}}\bar{q} + \bar{\rho}\overline{S}_T A_{\xi^a}\bar{q} \tag{45}$$

Each flow variable is normalized by its mean-flow quantity to yield

$$\frac{\dot{Q}^a}{\overline{\dot{Q}}} = \frac{q^a}{\bar{q}} + \frac{\rho^a}{\bar{\rho}} + \frac{S_T^a}{\overline{S}_T} + \frac{A_{\xi^a}}{A_{\bar{\xi}}} \tag{46}$$

Thus, the fluctuation of heat-release rate contains contributions from the fluctuations in heat of reaction, density, flame speed, and flame-surface area. The effects of each of those terms are discussed in the following subsections.

Fluctuation of Mixture Density

As a result of flow oscillations at the flame front, entropy fluctuations are generated and convected downstream. Thus, density can be conveniently expressed in terms of pressure and entropy.

$$\rho = \rho(p, s) \tag{47}$$

Linearization of this equation of state for a perfect gas leads to

$$\frac{\rho^a}{\bar{\rho}} = \frac{p^a}{\gamma \bar{p}} - \frac{s^a}{C_p} \tag{48}$$

where γ and C_p represent the specific heat ratio and the constant-pressure specific heat for the mixture, respectively. The density disturbance contains contributions from pressure fluctuations which propagate at the speed of sound and entropy fluctuations which are convected downstream with the mean flow.

Fluctuation of Heat of Reaction

For premixed flames, heat of reaction depends on mixture composition and heats of formation of the constituent species. Abu-Orf and Cant (1996) derived the following expression for a methane-air mixture in

terms of its equivalence ratio ϕ.

$$q(\phi) = \begin{cases} \dfrac{\phi \cdot 2.9125 \times 10^6}{1 + \phi \cdot 0.05825}, & \phi \le 1 \\ \dfrac{2.9125 \times 10^6}{1 + \phi \cdot 0.05825}, & \phi > 1 \end{cases} \quad (J/kg) \tag{49}$$

The fluctuation of the equivalence ratio often results from flow variations in the fuel/air mixer, and is responsible for the occurrence of low-frequency oscillations in several lean-premixed combustion systems (Cho and Lieuwen, 2003). Figure 12 shows a typical mixer in which fuel is injected from the centerbody spokes and mixed with the incoming air in the inlet annulus. Following the definition of the equivalence ratio and applying the averaging operations, we obtain the following linearized equation.

$$\frac{\phi^a}{\bar{\phi}} = \frac{\dot{m}^a_{fuel}}{\bar{\dot{m}}_{fuel}} - \frac{\dot{m}_{air}{}^a}{\bar{\dot{m}}_{air}} \tag{50}$$

For a choked fuel injector, $\dot{m}^a_{fuel} = 0$. Substitution of the air mass flow rate $\dot{m}_{air} = \rho u A_{in}$ into Eq. (50) yields

$$\frac{\phi^a}{\bar{\phi}} = -\left(\frac{u^a}{\bar{u}} + \frac{\rho^a}{\bar{\rho}}\right) \tag{51}$$

Since the mixture convected from the fuel injector plane will burn in the flame zone after a time delay τ_{conv} from its injection, a relationship can be

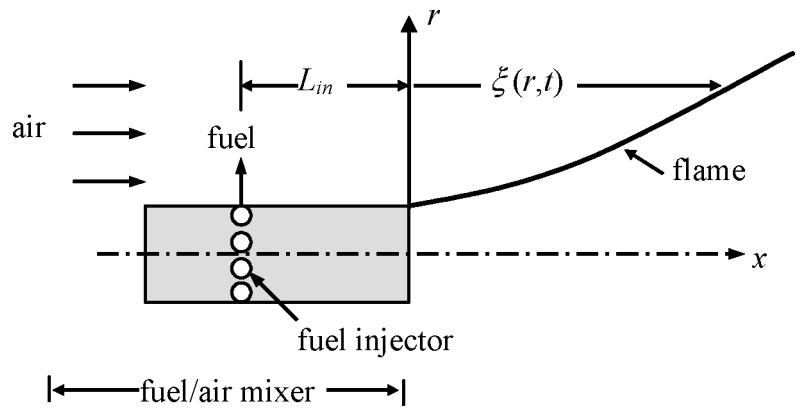

Figure 12. Schematic of fuel/air mixer and flame displacement.

established between the flame displacement and such a time lag (Fung et al., 1991).

$$\xi + L_{in} = \int_{t}^{t+\tau_{conv}} u(t,\tau)d\tau \tag{52}$$

where L_{in} measures the distance from the injector to the base of the flame holder. The integral is evaluated following the motion of the mixture element injected at t, and $u(t,\tau)$ is the velocity of the mixture element injected at t after an interval τ. Accordingly, the equivalence-ratio oscillation at the flame front for a time-harmonic disturbance becomes

$$\left[\frac{\phi^a}{\bar{\phi}}\right]_f = -\left[\frac{u^a}{\bar{u}} + \frac{\rho^a}{\bar{\rho}}\right]_{in} \exp(-i\Omega\tau_{conv}) \tag{53}$$

where the subscripts f and in represent variables evaluated at the flame front and injector, respectively. Although turbulent diffusion tends to homogenize the mixture as it flows downstream, this process is neglected here to simplify the formulation. In the limiting case with a constant particle velocity (i.e., $u(t,\tau) = \bar{u}$), a simple expression for the convective time delay is obtained as $\tau_{conv} = (L_{in} + \bar{\xi})/\bar{u}$.

For longitudinal acoustic waves, a flow disturbance of frequency Ω at the flame front can be related to that at the injector plane with a phase difference. If the mean-flow Mach number is small, the relationship becomes

$$\left.\frac{u^a}{\bar{a}}\right|_f = \left.\frac{u^a}{\bar{a}}\right|_{in} \exp\left[-i\Omega\left(L_{in} + \bar{\xi}\right)/\bar{a}\right] \tag{54}$$

where $\bar{a}$ is the speed of sound. Since the acoustic phase difference $\Omega(L_{in} + \bar{\xi})/\bar{a}$ is much smaller than that associated with flow convection, $\Omega\tau_{conv}$, the equivalence-ratio fluctuation can be derived by substituting Eq. (54) into (53).

$$\left.\frac{\phi^a}{\bar{\phi}}\right|_f = \left[\left.\frac{u^a}{\bar{u}}\right|_f \left(\frac{\overline{M}_f}{\overline{M}_{in}}\right) - \left.\frac{p^a}{\gamma\bar{p}}\right|_f\right] \exp(-i\Omega\tau_{conv}) \tag{55}$$

The fluctuation in the heat of reaction can be described in the following form, where the difference between the Mach number at the flame front $\overline{M}_f$ and the fuel injector $\overline{M}_{in}$ is ignored.

$$q^a = \left.\frac{dq}{d\phi}\right|_{\bar{\phi}} \bar{\phi}\left(\frac{u^a}{\bar{u}} - \frac{p^a}{\gamma\bar{p}}\right) \exp(-i\Omega\tau_{conv}) \tag{56}$$

Fluctuation of Flame Speed

According to Eq. (42), the turbulent flame speed S_T arises from the ensemble-averaged correlation between the laminar flame speed and flame surface area. In general S_T is a function of the laminar flame speed S_L, flame thickness l_F, turbulent velocity fluctuation v', turbulent integral length scale l, and other parameters.

$$S_T = f(S_L, l_F, v', l, \ldots) \tag{57}$$

For a given set of chamber conditions and flow environment, the sensitivity of turbulent flame speed to impressed acoustic fluctuations can be related to its laminar counterpart, provided the flame thickness is much smaller than the acoustic wavelength. The laminar flame speed S_L depends on the local equivalence ratio ϕ, pressure p, and temperature T as follows (Abu-Orf and Cant, 2000).

$$S_L(\phi, T, P) = A\phi^B \exp\left[-C(\phi - D)^2\right](T/T_0)^\alpha (p/p_0)^\beta \tag{58}$$

For premixed methane-air mixtures, the coefficients are $A = 0.6079\,\mathrm{m/s}$, $B = -2.554$, $C = 7.31$, $D = 1.23$, $\alpha = 2$, and $\beta = -0.5$, with $p_0 = 1\,\mathrm{bar}$ and $T_0 = 300\,\mathrm{K}$.

The individual effects of the fluctuating equivalence ratio, pressure, and temperature on the flame speed can be evaluated in accordance with Eq. (58) as

$$(\partial S_L/\partial\phi)|_{\bar{\phi}} \cdot \phi^a = \left[B - 2\bar{\phi}C\left(\bar{\phi} - D\right)\right]\overline{S}_L\left(\phi^a/\bar{\phi}\right) \tag{59}$$

$$(\partial S_L/\partial p)|_{\bar{p}} \cdot p^a = \beta\overline{S}_L(p^a/\bar{p}) \tag{60}$$

$$(\partial S_L/\partial T)|_{\overline{T}} \cdot T^a = \alpha\overline{S}_L\left(T^a/\overline{T}\right) \tag{61}$$

Following the analysis described in the previous section, the equivalence-ratio fluctuation is related to the acoustic disturbance at the flame front, and the following equation is produced.

$$\left.\frac{\partial S_L}{\partial\phi}\right|_{\bar{\phi}} \phi^a = \left[B - 2\bar{\phi}C\left(\bar{\phi} - D\right)\right]\overline{S}_L\left(\frac{\boldsymbol{u}^a}{\bar{\boldsymbol{u}}} - \frac{p^a}{\gamma\bar{\boldsymbol{p}}}\right)e^{-i\Omega\tau_{conv}} \tag{62}$$

An order-of-magnitude analysis is performed to assess the pressure and temperature sensitivities of the flame speed. First, the pressure disturbance in Eq. (60) is expressed as the product of velocity perturbation

and acoustic impedance $\overline{\rho a}$, giving

$$\left.\frac{\partial S_L}{\partial p}\right|_{\bar{p}} p^a \propto \beta \overline{S}_L \overline{M} \gamma \frac{u^a}{\bar{u}} \tag{63}$$

Similarly, the temperature disturbance can be written in terms of the velocity perturbation through the use of the isentropic relationship between the temperature and pressure fields. As a result, Eq. (61) becomes

$$\left.\frac{\partial S_L}{\partial T}\right|_{\overline{T}} T^a \propto \alpha \overline{S}_L \overline{M} (\gamma - 1) \frac{u^a}{\bar{u}} \tag{64}$$

The above equations indicate that the effects of temperature and pressure disturbances are one order of $\overline{M}$ greater than that of the equivalence-ratio oscillation. For low-speed flows, such as those encountered in most gas-turbine combustors, the flame-speed fluctuation becomes

$$S_L^a = \left(\frac{\partial S_L}{\partial \phi}\right)\bigg|_{\bar{\phi}} \bar{\phi}\left[\left.\frac{u^a}{\bar{u}}\right|_f - \left.\frac{p^a}{\gamma \bar{p}}\right|_f\right] \exp(-i\Omega\tau_{conv}) \tag{65}$$

Fluctuation of Flame Surface Area

The mean and acoustic-wave-augmented flame surface areas, $A_{\bar{\xi}}$ and A_{ξ^a}, can be obtained by substituting the displacement function derived in Eqs. (21) and (22) into Eq. (23), as shown below.

$$\begin{aligned} A_{\bar{\xi}} &= \frac{1}{\Delta x}\sqrt{\left(d\bar{\xi}/dr\right)^2 + 1} \\ A_{\xi^a} &= \frac{1}{\Delta x}\left\{\sqrt{\left[\partial\left(\bar{\xi} + \xi^a\right)/\partial r\right]^2 + 1} - \sqrt{\left(d\bar{\xi}/dr\right)^2 + 1}\right\} \end{aligned} \tag{66}$$

Since it has been shown that Eq. (33) is a good approximation for the overall flame response to acoustic disturbances, the same approach is used to formulate the local flame response. The result becomes

$$\frac{A_{\xi^a}}{A_{\bar{\xi}}} = \frac{u_n^a \sin\alpha \cos\alpha}{\overline{U}_\alpha} \exp\left[\frac{-i\Omega(r - R_i)}{\overline{U}_\alpha}\right] \tag{67}$$

Combustion Response Function

The fluctuating quantities derived above, Eqs. (48), (56), (65), and Eq. (67), are substituted into Eq. (46) to determine the response of

heat-release rate to impressed disturbances. The result can be conveniently related to local pressure and velocity fluctuations to facilitate the establishment of a general framework for predicting the combustion stability characteristics of an engine. Following common practice, the normalized rate of heat release is written as

$$\frac{\dot{Q}'}{\overline{\dot{Q}}} = R_p \frac{p^a}{\bar{p}} + R_u \frac{u^a}{\bar{u}} + R_v \frac{v^a}{\bar{v}} + R_w \frac{w^a}{\bar{w}} \tag{68}$$

where R_p and R_u, R_v, and R_w are complex variables commonly referred to as the pressure- and velocity-coupled response functions. After some straightforward manipulations, we have

$$\begin{aligned} R_p(r) &= \underbrace{\frac{1}{\gamma}}_{\text{group I}} \underbrace{-\frac{1}{\gamma} f_\phi e^{-i\Omega\left(\frac{(r-R_i)\tan\alpha}{\bar{u}}+\tau_0\right)}}_{\text{group II}} \\ R_u(r) &= \underbrace{-f_\phi e^{-i\Omega\tau_{conv}}}_{\text{group II}} + \underbrace{\frac{\bar{u}\sin\alpha\cos\alpha}{\overline{U}_\alpha} e^{\frac{-i\Omega(r-R_i)}{\overline{U}_\alpha}}}_{\text{group III}} \\ R_v(r) &= \underbrace{-\frac{\bar{v}\sin^2\alpha}{\overline{U}_\alpha} \exp\left(\frac{-i\Omega(r-R_i)}{\overline{U}_\alpha}\right)}_{\text{group III}} \end{aligned} \tag{69}$$

where

$$f_\phi = (\partial S_L/\partial\phi)|_{\bar{\phi}}\left(\bar{\phi}/\overline{S}_L\right) + (dq/\partial\phi)|_{\bar{\phi}}\left(\bar{\phi}/\bar{q}\right)$$

The effect of azimuthal velocity fluctuation is ignored due to its minor influence in an axisymmetric configuration.

Acoustic oscillations modify both the heat of reaction and mass burning rate of a mixture. The influence on heat of reaction is exerted through the changes in the mixture-equivalence ratio, and most likely is important in the low-frequency range. The variation of the mass burning rate in the flame zone results from the fluctuations in the mixture density, flame speed, and specific flame surface area. Among these three quantities, the density fluctuation, mainly arising from pressure perturbations, has a negligible effect on unsteady heat release as compared to the latter two. The oscillation of flame speed, similar to that of heat of reaction, is also caused by the equivalence-ratio fluctuation for a given chamber and flow environment. The mechanisms of flame surface area fluctuations are relatively complicated and primarily dictated by local velocity perturbations. Figure 13 illustrates these contributions to

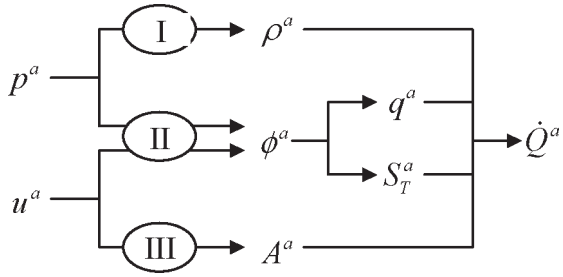

Figure 13. Effects of acoustic disturbances on unsteady heat release.

unsteady heat release, where I, II, and III refer to the group numbers in Eq. (69). The combustion response given in Eq. (69) can hence be classified into three groups according to the specific driving mechanisms involved. The first group represents the density-fluctuation effect. The second group describes the effects of flame-speed and heat-of-reaction oscillations on unsteady heat-release fluctuation due to the equivalence-ratio disturbance. The third group characterizes the influence of acoustic velocity on the flame-surface area. These coefficients are mainly functions of acoustic frequency, local flow and flame velocities, and sensitivities of heat of reaction and flame speed to the equivalence ratio. The contribution of each individual mechanism can be examined from its frequency-response behavior.

If the flame is acoustically compact, with its length much smaller than the acoustic wavelength, it is instructive to examine the global combustion response of the entire flame by integrating the local response over the entire flame zone. Such information provides direct insight into the combustion sensitivity to acoustic excitation, especially for low-frequency oscillations such as bulk and longitudinal modes. Assuming constant pressure and axial velocity fluctuations in the flame zone, we obtain the following global combustion response functions.

pressure-coupled response

$$
\begin{aligned}
R_p^g &= \left(R_p^g\right)_\rho + \left(R_p^g\right)_\phi \\
\left(R_p^g\right)_\rho &= \frac{1}{\gamma} \\
\left(R_p^g\right)_\phi &= -\frac{2(R_c - R_i)}{\gamma(R_c + R_i)} f_\phi \frac{e^{-i\Omega\tau_0}}{\Omega_\phi^2}\left[e^{-i\Omega_\phi}(1 + i\Omega\tau_2) - (1 + i\Omega\tau_1)\right]
\end{aligned}
\tag{70}
$$

velocity-coupled response

$$
\begin{aligned}
R_u^g &= \left(R_u^g\right)_\phi + \left(R_u^g\right)_u \\
\left(R_u^g\right)_\phi &= \frac{2(R_c - R_i)}{R_c + R_i} f_\phi \frac{e^{-i\Omega\tau_0}}{\Omega_\phi^2}\left[e^{-i\Omega_\phi}(1 + i\Omega\tau_2) - (1 + i\Omega\tau_1)\right] \\
\left(R_u^g\right)_u &= \frac{R_c - R_i}{R_c + R_i}\frac{\bar{u}\sin 2\alpha}{\Omega_f^2 \overline{U}_\alpha}\left[\left(\frac{i\Omega_f R_c}{R_c - R_i} + 1\right)\left(1 - e^{-i\Omega_f}\right) - i\Omega_f\right]
\end{aligned}
\tag{71}
$$

where $\tau_1 = R_i \tan\alpha/\bar{u}$ and $\tau_2 = R_c \tan\alpha/\bar{u}$. The subscripts ρ, ϕ, and u refer to the contributions from the fluctuations in the mixture density, equivalence ratio, and flow velocity, respectively. Only the axial velocity fluctuation is considered in the above formulation due to the underlying assumption (i.e., acoustic compactness of the flame) employed in deriving Eqs. (70) and (71). The difference between τ_1 and τ_2 lies in the flow convection time $L_f/\bar{u}$, where L_f is the flame length in the axial direction, given by $L_f = (R_c - R_i)\tan\alpha$. A dimensionless frequency Ω_ϕ associated with the equivalence-ratio fluctuation is defined as

$$\Omega_\phi = \Omega L_f/\bar{u} \tag{72}$$

Comparison of the coefficients in Eqs. (70) and (71) yields the following relationship.

$$\left(R_p^g\right)_\phi = \left(R_u^g\right)_\phi \cdot (-1/\gamma) \tag{73}$$

Thus, the pressure- and velocity-coupling effects are closely related to each other in this limiting case.

Figure 14 shows the magnitudes and phases of $\left(R_u^g\right)_\phi$, $\left(R_u^g\right)_u$, and the overall response, R_u^g, as a function of the flame Strouhal number Ω_f. The combustion response has its maximum value at zero frequency, and decays with increasing frequency. Since the coefficient $\left(R_u^g\right)_\phi$ is much larger than $\left(R_u^g\right)_u$, the dominant effect on unsteady heat release is caused by the equivalence-ratio fluctuation. This behavior may be attributed to the increased sensitivity of the flame speed and heat of reaction to the equivalence ratio for lean premixed mixtures. The same phenomenon was also observed by Hubbard and Dowling (1998) and Lieuwen (2003). Owing to the dominance of $\left(R_u^g\right)_\phi$, the phase of the total response function R_u^g follows that of $\left(R_u^g\right)_\phi$. The constant convection times τ_0, τ_1, and τ_2 give rise to a saw-tooth distribution in the phase diagram.

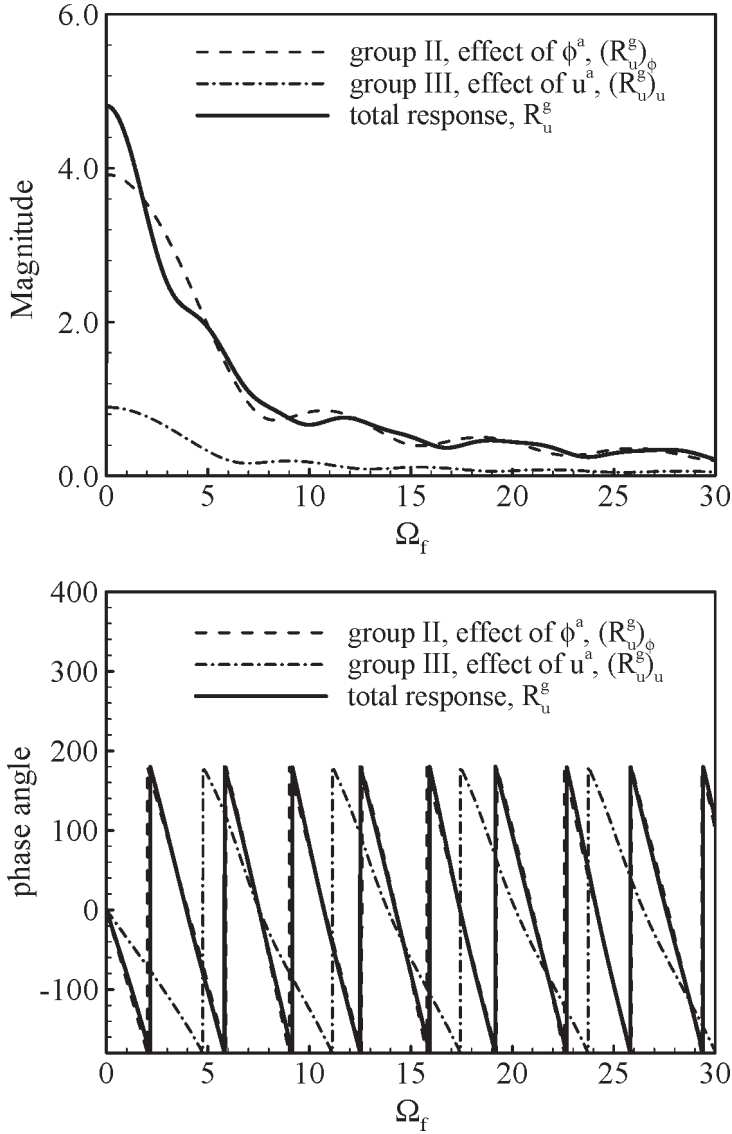

Figure 14. Magnitude and phase angle of velocity-coupled combustion response to acoustic oscillation as function of flame Strouhal number Ω_f (simple flame).

In a swirl-stabilized combustor, an enveloped flame, as shown schematically in Fig. 3(b), may develop under certain operating conditions (Huang et al., 2003). The dynamics of such a flame are determined by the combined effect of the upper and lower branches, and no single characteristic frequency can be defined. Following the procedure leading to Eqs. (70) and (71) for a simple flame, the combustion response functions of an enveloped flame can be derived by separately integrating the rate of heat release over the two branches of the flame zone. The explicit forms are summarized below.

$$\begin{aligned} R_p^g &= \left(R_p^g\right)_\rho + \left(R_p^g\right)_\phi \\ \left(R_p^g\right)_\rho &= \frac{1}{\gamma} \\ \left(R_p^g\right)_\phi &= -\frac{\bar{u}^2 f_A f_\phi \exp(-i\Omega\tau_0)}{\gamma}\left(\frac{\cos\beta}{\sin\alpha}f_a + \frac{\cos\alpha}{\sin\beta}f_\beta\right) \end{aligned} \tag{74}$$

where

$$\begin{aligned} f_A &= \frac{2}{\Omega^2\left[\cos\beta\left(R_t^2 - R_i^2\right) + \cos\alpha\left(R_t^2 - R_o^2\right)\right]} \\ f_\alpha &= \left[e^{-i\Omega\bar{\xi}(R_t)/\bar{u}}\left(i\Omega\tau_1 + i\Omega\bar{\xi}(R_t)/\bar{u} + 1\right) - (1 + i\Omega\tau_1)\right] \\ f_\beta &= \left[e^{-i\Omega\bar{\xi}(R_t)/\bar{u}}\left(i\Omega\tau_2 + i\Omega\bar{\xi}(R_t)/\bar{u} + 1\right) - (1 + i\Omega\tau_2)\right] \end{aligned}$$

The radial coordinate of the long-time-averaged flame tip is denoted by R_t.

$$\begin{aligned} R_u^g &= \left(R_u^g\right)_\phi + \left(R_u^g\right)_u \\ \left(R_u^g\right)_\phi &= -\bar{u}^2 f_A f_\phi e^{-i\Omega\tau_0}\left(\frac{M_f}{M_{in}}\right)\left(\frac{\cos\beta}{\sin\alpha}f_a + \frac{\cos\alpha}{\sin\beta}f_\beta\right) \\ \left(R_u^g\right)_u &= -\bar{u}\cos\alpha\cos\beta f_A \\ &\quad \times \left[\begin{array}{l} \sin\alpha\left(i\Omega R_i + \overline{U}_\alpha - \left(i\Omega R_t + \overline{U}_\alpha\right)e^{-i\Omega(R_t - R_i)/\overline{U}_\alpha}\right) \\ + \sin\beta\left(i\Omega R_o + \overline{U}_\beta - \left(i\Omega R_t + \overline{U}_\beta\right)e^{-i\Omega(R_t - R_o)/\overline{U}_\beta}\right) \end{array}\right] \end{aligned} \tag{75}$$

Figure 15 shows the magnitudes of the combustion-response coefficients of the enveloped flame as a function of Ω_f, based on the properties of the lower branch. The response function decays with increasing frequency, as in the simple-flame case, but with a much higher $\left(R_u^g\right)_\phi$. It reaches around 8.5 at zero frequency, indicating that the effect of the equivalence-ratio fluctuation is much stronger for this enveloped flame

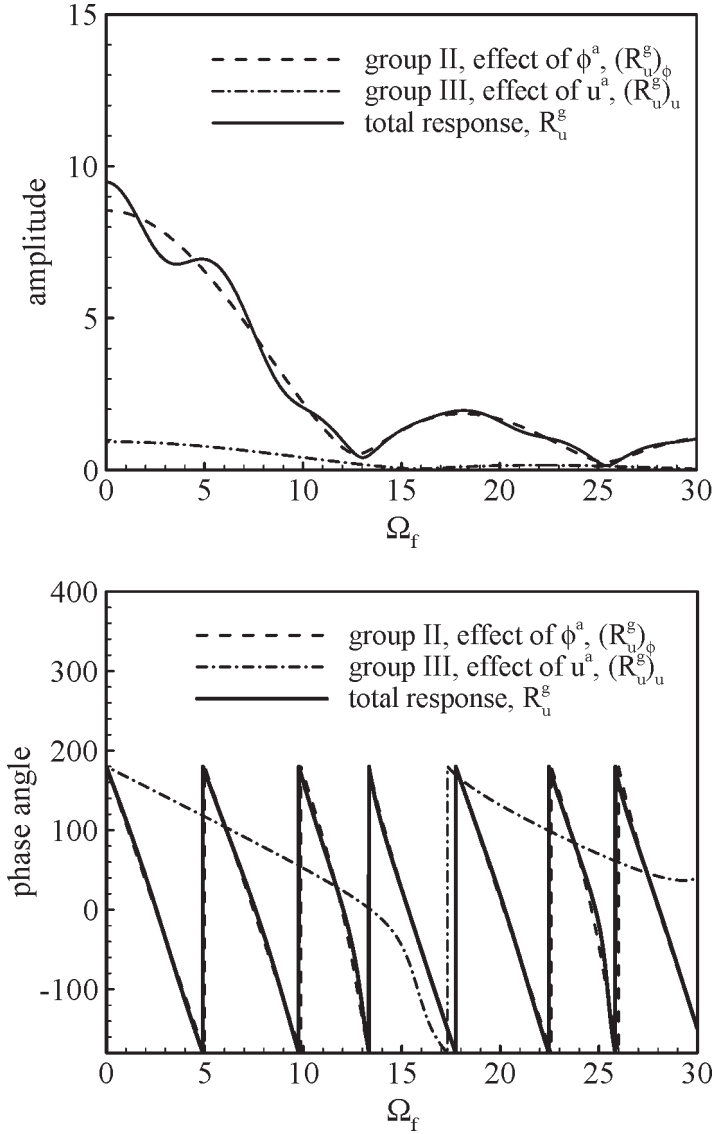

Figure 15. Magnitude and phase angle of velocity-coupled combustion response to acoustic oscillation as function of flame Strouhal number Ω_f (enveloped flame).

configuration. The phase of $\left(R_u^g\right)_\phi$ also shows a sawtooth shape, and dictates the phase behavior of the total response function.

COMBUSTION INSTABILITY OF GAS TURBINE ENGINE

Three-Dimensional Instability Analysis

The combustion response functions derived in the preceding section can be effectively incorporated into a three-dimensional linear acoustic analysis of combustion instabilities in gas-turbine engines (You et al., 2003). The analysis is capable of treating both longitudinal and transverse waves as well as their combinations in complex configurations with nonuniform distributions of mean-flow properties. In brief, it can be constructed in several steps. First, a generalized wave equation governing the oscillatory field in the chamber is derived,

$$\nabla^2 p^a - \frac{1}{\bar{a}^2}\frac{\partial^2 p^a}{\partial t^2} = h\left(\bar{\boldsymbol{u}}, \bar{p}, \boldsymbol{u}^a, p^a, \dot{\boldsymbol{Q}}^a, \text{etc.}\right) \tag{76}$$

subject to $\boldsymbol{n}\cdot\nabla p^a = -f$ along the boundary. The source terms h and f involve all the volumetric and surface effects. To account for spatial variations of the chamber geometry and mean flow field, the combustor is discretized axially into a number of cells, as shown in Figure 16, such that the mean axial flow properties within each cell can be taken to be uniform. Furthermore, the mean-flow Mach number on the transverse plane is assumed to be small, as in most practical combustion systems. The acoustic field in each cell is synthesized as a Fourier-type series in terms of the eigenfunctions for the cross section, but allows for temporal and axial variations through the series coefficients. In cylindrical coordinates, this can be expressed as

$$p^a(\boldsymbol{r}, t) = \sum_{n=0}^{\infty}\sum_{m=-\infty}^{\infty}\left[\psi_{mn}(\theta, r)\eta_{mn}(x, t)\right] \tag{77}$$

The eigenfunction ψ_{mn} can be well approximated by that of a classical acoustic field without source terms. It satisfies the Helmholtz equation for the transverse plane and is subject to the homogeneous boundary condition along the combustor wall. The subscripts m and n stand for mode indices in the circumferential and radial directions, respectively. After expansion, a spatial-averaging technique is applied to solve for the axial variation of the acoustic field.

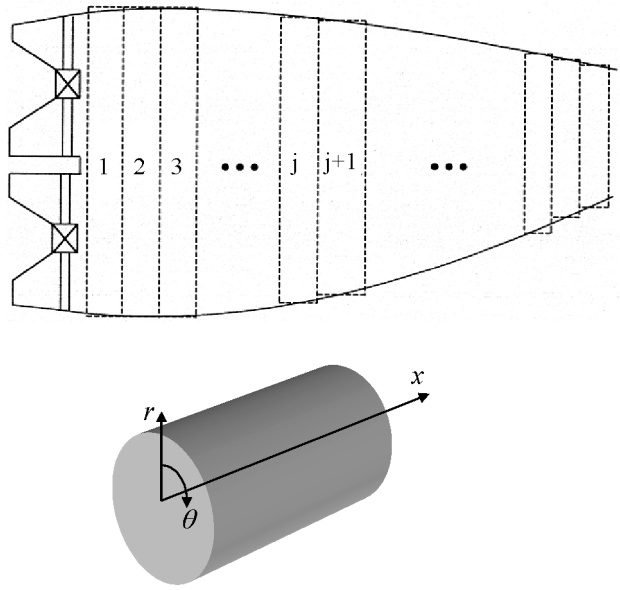

Figure 16. Discretization of combustion chamber length into cells in the axial direction.

The volumetric and boundary processes appearing on the right-hand side of the wave equation must be modeled. To facilitate formulation, the coefficients C_h and C_f are introduced to represent these terms, as shown below.

$$\iint \psi_{mn}\hat{\boldsymbol{h}}\boldsymbol{ds} = C_{h,mn}\hat{\eta}_{mn}(x)$$
$$\oint \psi_{mn}\hat{\boldsymbol{f}}_T\boldsymbol{dl} = C_{f,mn}\hat{\eta}_{mn}(x) \tag{78}$$

The source term arising from oscillatory combustion can be written as

$$\boldsymbol{h} = -i\Omega\dot{\boldsymbol{Q}}^a(\gamma - 1)/\bar{\boldsymbol{a}}^2 \tag{79}$$

Substituting Eq. (79) into Eq. (78), and applying the response function derived in the previous section, the coefficient $C_{h,mn}$ is obtained as

$$G^{\pm}_{h,mn} = \iint \psi_{mn} G^{\pm}_{h,mn}\boldsymbol{ds} \tag{80}$$

where

$$G^{\pm}_{hmn} = -\frac{i(\gamma-1)\Omega\overline{Q}}{\bar{\rho}\bar{a}^2}\cdot\left[\frac{R_p\bar{\rho}}{\bar{p}}\psi_{mn} - \frac{R_u\alpha^{\pm}_{mn}\psi_{mn}}{\bar{u}(\Omega+\bar{u}\alpha^{\pm}_{mn})} + \frac{iR_v}{\bar{v}(\Omega+\bar{u}\alpha^{\pm}_{mn})}\frac{\partial\psi_{mn}}{\partial r}\right]$$

After modeling the various source terms in the wave equation, the acoustic pressure field in each cell can be solved in the following form.

$$p^a(\boldsymbol{r},t) = \mathrm{e}^{i\Omega t}\sum_{n=0}^{\infty}\sum_{m=-\infty}^{\infty}[\psi_{mn}(\theta,r)\hat{\eta}_{mn}(x)] \tag{81}$$

where

$$\hat{\eta}_{mn}(x) = p^{+}_{mn}\exp\left(i\alpha^{+}_{mn}x\right) + p^{-}_{mn}\exp\left(i\alpha^{-}_{mn}x\right)$$

The axial wave number α_{mn} is given by

$$\left(\alpha^{\pm}_{mn}\right)^2 = \left(\Omega^2/\bar{a}^2\right) - k^2_{mn} - C_{h,mn} - C_{f,mn} \tag{82}$$

where Ω denotes the oscillation eigenfrequency, and k_{mn} is the eigenvalue corresponding to the transverse eigenfunction ψ_{mn}.

The oscillatory flow properties in each cell are matched with those in the adjacent cells at the cell interfaces by enforcing the conservation laws. The procedure eventually leads to a system equation which determines the stability characteristics and spatial structure of the acoustic waves in the entire system. The resultant characteristic frequency Ω is complex.

$$\Omega = \Omega_r + i\Omega_i \tag{83}$$

The real part Ω_r is the radian frequency, and the imaginary part Ω_i is referred to as the damping coefficient because its value determines the decay rate of a particular acoustic mode. Compared with conventional numerical methods, the present analysis is compact and efficient, and can be effectively used to investigate gas-turbine combustion instability.

Acoustic Instability in Swirl-Stabilized Combustor

As a specific example, we consider a lean-premixed swirl-stabilized combustor typical of gas-turbine applications, as shown schematically in Figure 1. The model includes an axisymmetric chamber connected upstream with an inlet annulus, which houses a swirler and a fuel injection unit, and downstream with a choked nozzle, simulating the experimental

facility operated by Broda et al. (1998). The baseline condition includes an equivalence ratio of 0.573, and a chamber pressure of 0.463 MPa. The mass flow rates of the natural gas and air are 1.71 and 50.70 g/s, respectively. The inlet flow velocity is 86.6 m/s and the corresponding Reynolds number based on the inlet flow velocity and height of the inlet annulus is 35,000. Combustion instability occurs when the inlet air temperature exceeds a threshold value and the equivalence ratio falls into a certain range. More detailed information about the experimental observations can be found in the paper by Broda et al. (1998). The underlying mechanisms for driving instabilities were studied by Huang et al. (2003) and Huang and Yang (2004) using a large-eddy-simulation (LES) technique.

Based on the experimental and numerical results, two cases are investigated in the present study. Case 1 is associated with a stable operating condition with an inlet temperature of 600 K, and Case 2 corresponds to an unstable situation with an inlet temperature of 660 K. Figure 17 shows the mean-temperature contours and streamlines on a

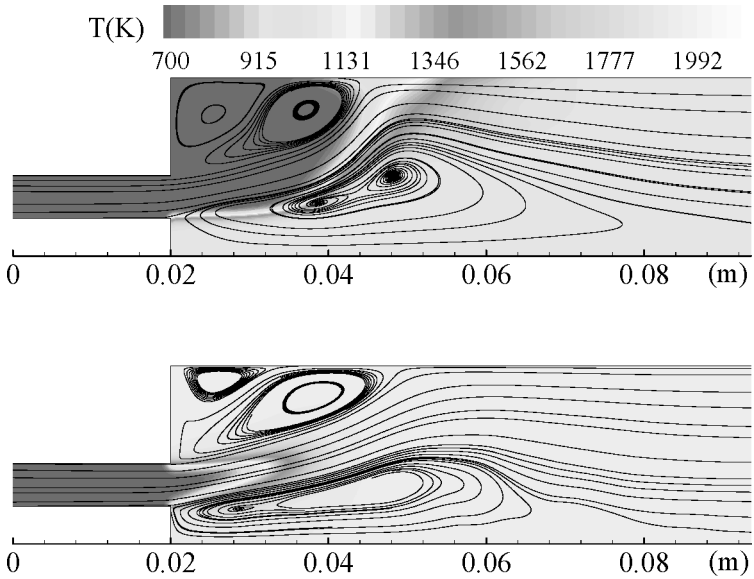

Figure 17. Mean temperature contours and streamlines in swirl-stabilized combustor (Huang, et al., 2003; Huang and Yang, 2004), *top*: simple flame ($T_{\text{in}} = 600\,\text{K}, \text{S} = 0.76$, $\bar{\phi} = 0.57$, $\bar{p} = 0.463$ MPa), *bottom*: enveloped flame ($T_{\text{in}} = 600\,\text{K}, \text{S} = 0.76, \bar{\phi} = 0.57$, $\bar{p} = 0.463$ MPa). (See Color Plate 13 at the end of this issue).

longitudinal plane for the two cases, obtained from the LES analysis (Huang and Yang, 2004). A central toroidal recirculation zone and a corner recirculation zone exist in both cases due to the swirling effect of the inlet flow. In Case 1, the flame spreads from the corner of the center body to the chamber wall. In Case 2, the flame is anchored by both the corner and the center recirculating flows and forms a compact enveloped configuration, which is in sharp contrast with the stable flame structure. The flames in these two cases can be modeled as a simple and an enveloped flame, respectively.

The average flame-spreading angles α and β can be estimated from the calculated mean-temperature fields. A value of $\alpha = 60^\circ$ is used in the simple-flame case, and $\alpha = 68^\circ$ and $\beta = 83^\circ$ are used in the enveloped-flame case. These quantities along with the mean-flow properties are substituted into Eq. (69) to determine the combustion response function, which is then employed in the generalized acoustic analysis, as outlined in Section 4.1, to characterize the stability behavior of the combustor.

Table 1 summarizes the calculated oscillation frequencies and damping coefficients of the first longitudinal (1L), first tangential (1 T), and first radial (1 R) modes for both cases. The results agree well with the experimental observations (Broda et al., 1998) and LES calculations (Huang et al., 2003). For the enveloped flame (Case 2), the calculated frequency of 1753 Hz matches closely the experimental value of 1750 Hz. The spatial distribution of the first longitudinal mode shown in Figure 18 also demonstrates the validity of the present analysis.

The occurrence of the unstable 1L mode in the enveloped flame case can be explained by the coupling between the unsteady heat release and pressure oscillations. When the inlet air temperature is increased from

Table 1. Calculated oscillation frequencies and damping coefficients for a swirl-stabilized combustor

	Case 1 ($T_{in} = 660$ K)		Case 2 ($T_{in} = 660$ K)	
Mode	Frequency (Hz)	Damping coefficient (s^{-1})	Frequency (Hz)	Damping coefficient (s^{-1})
1L	1645	2.1	1753	−21
1T	10610	0.9	11310	−3.3
1R	22297	3.5	24236	−4.5

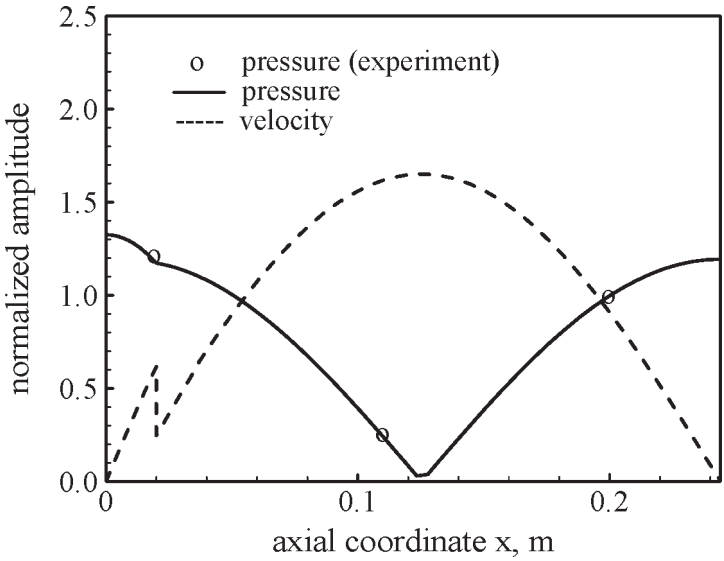

Figure 18. Distributions of acoustic oscillations in swirl-stabilized combustor, first longitudinal mode.

600 K to 660 K, the near-wall flashback overshadows the flow acceleration effect with the aid of the increased flame speed. As a result, the flame penetrates into the corner recirculation zone and is trapped by the local vortical motion. The flame is thus stabilized by both the corner- and center-recirculating flows. The overall flame is substantially reduced, and more energy is released near the chamber head-end. Since this location corresponds to the pressure anti-node of the 1L mode, the acoustic oscillation can be easily excited according to Rayleigh's criterion.

The excitation of combustion instability in the enveloped flame case is also reflected in the global combustion response. For the simple flame case, the flame Strouhal number Ω_f of the first longitudinal mode is 6.52, which gives an amplitude of 1.27 and a phase angle of 109 degrees for the combustion response function. The corresponding quantities for the enveloped flame case are 7.43 and –30 degrees, respectively. Since the unsteady heat release adds energy to the oscillatory field only when the phase of the response function R_u^g is negative, the higher amplitude and the negative phase lag for an enveloped flame tend to drive and sustain instabilities according to Rayleigh's criterion. These results further validate the combustion-response function derived in the present study.

CONCLUSIONS

An analytical model has been developed to study the transient combustion response of a premixed turbulent flame to acoustic oscillation. The analysis takes into account all factors affecting the flame dynamics, and accommodates the effects of spatial variations in chamber geometry and mean flow field. The resultant response function was incorporated into a three-dimensional acoustic analysis to investigate the oscillatory flow characteristics of a combustion chamber. As a specific example, the stability behavior of a swirl-stabilized combustor was treated. Good agreement is achieved between the analytical results and experimental data.

NOMENCLATURE

A	flame surface area density
$\bar{a}$	speed of sound in mixture
C_f, C_h	coefficient of source term model, Eq. (78)
C_r	coefficient, defined as $C_r = \overline{S}_T/(\bar{u}\cos\alpha) - 1$
f	boundary condition, Eq. (76)
G	flame surface scalar variable
h	source term in wave equation, Eq. (76)
i	$\sqrt{-1}$
k	flame front curvature
k_{mn}	eigenvalue of mnth mode
L_{in}	length of inlet annulus after injector plane
l	perimeter of cross section
l_F	flame thickness
$\dot{m}$	mass consumption rate of mixture per unit volume
M	mean-flow Mach number
$\boldsymbol{n}$	unit vector normal to flame front, or unit vector normal to chamber surface
p	pressure
q	heat of reaction per unit mass of the mixture
$\dot{Q}$	rate of heat release
R_c	radius of combustion chamber
$R_i,\ R_o$	inner and outer radius of annular inlet
$R_p,\ R_u,\ R_v,\ R_w$	combustion response coefficient, Eq. (68)
R_t	radius of enveloped flame tip
$\boldsymbol{r}$	position vector
r	radial coordinate

S	Swirl number
S_L	laminar flame speed
S_T	turbulent flame speed
s	entropy
T	temperature
t	time
$\boldsymbol{u}$	mixture velocity vector
u	axial velocity
v	radial velocity
w	circumferential velocity
x	axial coordinate

Greek Letters

α, β	flame-spreading angle, Fig. 3
α	axial wave number
ρ	mixture density
φ_u	phase of acoustic velocity
φ_g	phase of flame-surface fluctuations
ϕ	equivalence ratio
ψ	normal mode function
θ	circumferential coordinate
ξ	flame surface displacement
γ	specific heat ratio for mixture
Ω	radian frequency
Ω_{u}	dimensionless frequency, Eq. (72)
Ω_ϕ	dimensionless frequency, Eq. (25)
τ	period of oscillation
τ_{conv}	convection time
ν_t	turbulent viscosity

Overscripts

–	mean quantity
$'$	perturbation quantity
$\wedge$	fluctuation amplitude
$<>$	ensemble average

Superscripts

a	periodical component
g	response of entire flame
t	turbulent component

Subscripts

f	flame
i	imaginary part
in	fuel injection plane
m	circumferential direction mode
n	radial direction mode
r	real part

REFERENCES

Abu-Orf, G.M. and Cant, R.S. (1996) Reaction rate modeling for premixed turbulent methane-air flames. *Proc. of the Joint Meeting of the Spanish, Portuguese, Swedish and British Sections of the Combust. Inst.*

Abu-Orf, G.M. and Cant, R.S. (2000) A turbulent reaction rate model for premixed turbulent combustion in spark-ignition engines. *Combust. Flame*, **122**, 233–252.

Apte, S. and Yang, V. (2002) Unsteady flow evolution in porous chamber with surface mass injection, part 2: Acoustic excitation. *AIAA J.*, **40**, 244–253.

Broda, J.C., Seo, S., Santoro, R.J., Shirhattikar, G., and Yang, V. (1998) An experimental study of combustion dynamics of a premixed swirl injector. *Proc. Combust. Inst.*, **27**, 1849–1856.

Cho, J.H. and Lieuwen, T. (2003) Modeling the response of premixed flames to mixture ratio perturbations. *ASME Paper*, GT2003-38089.

Dowling, A.P. (1999) A kinematic model of a ducted flame. *J. Fluid Mech.*, **394**, 51–72.

Dowling, A.P. and Stow, S.R. (2003) Acoustic analysis of gas turbine combustors. *J. Prop. Power*, **19**, 751–764.

Eggenspieler, G. and Menon, S. (2004) Structure of locally quenched swirl stabilized turbulent premixed flames. *AIAA Paper*, 2004–0979.

Fleifil, M., Annaswamy, A.M., Ghoneim, Z.A., and Ghoniem, A.F. (1996) Response of a laminar premixed flame to flow oscillations: A kinematic model and thermoacoustic instability results. *Combust. Flame*, **106**, 487–510.

Fung, Y., Yang, V., and Sinha, A. (1991) Active control of combustion instabilities with distributed actuators. *Combust. Sci. Technol.*, **78**, 217–245.

Hsiao, G.C., Pandalai, R.P., Hura, H.S., and Mongia, H.C. (1998) Combustion dynamic modeling for gas turbine engines. *AIAA Paper*, 1998–3381.

Huang, Y. (2003) Modeling and Simulation of Combustion Dynamics in Lean-Premixed Swirl-Stabilized Gas-Turbine Engines. Ph.D. Thesis, Department of Mechanical Engineering, Pennsylvania State University.

Huang, Y., Sung, H., Hsieh, S., and Yang, V. (2003) Large-eddy simulation of combustion dynamics of lean-premixed swirl-stabilized combustor. *J. Prop. Power*, **19**, 782–794.

Huang, Y. and Yang, V. (2004) Bifurcation of flame structure in a lean-premixed swirl-stabilized combustor: transition from stable to unstable flame. *Combust. Flame*, **136**, 383–389.

Hubbard, S. and Dowling, A.P. (1998) Acoustic instabilities in premix burners. *AIAA Paper*, 1998–2272.

Hussain, A.K.M.F. and Reynolds, W.C. (1970) The mechanics of organized wave in turbulent shear flow. *J. Fluid Mech.*, **41**, 241–258.

Kerstein, A.R., Ashurst, W.T., and Williams, F.A. (1988) Field equation for interface propagation in an unsteady homogeneous flow field. *Phys. Rev. A*, **37**, 2728–2731.

Lieuwen, T. (2002) Analysis of acoustic wave interactions with turbulent premixed flames. *Proc. Combust. Inst.*, **29**, 1817.

Lieuwen, T. (2003) Modeling premixed combustion-acoustic wave interactions: A review. *J. Prop. Power*, **19**, 765–781.

Lieuwen, T. and McManus, K. (2003) Combustion dynamics in lean-premixed prevaporized (LPP) gas turbines. *J. Prop. Power*, **19**, 721.

Liñán, A. and Williams, F.A. (1993) *Fundamental Aspects of Combustion*, Oxford University Press, New York.

Liu, J.T.C. (1989) Coherent structures in transitional and turbulent free shear flows. *Ann. Rev. Fluid Mech.*, **21**, 285–315.

Marble, F.E. and Candel, S.M. (1978) An analytical study of the nonsteady behavior of large combustors. *Proc. Combust. Inst.*, **17**, 761–769.

Peters, N. (2000) *Turbulent Combustion*, Cambridge University Press, Cambridge, pp. 78–87.

Poinsot, T. and Candel, S.M. (1988) A nonlinear model for ducted flame combustion instabilities. *Combust. Sci. Technol.*, **61**, 121–151.

Poinsot, T., Veynante, D., and Candel, S. (1991) Quenching process and premixed turbulent combustion diagram. *J. Fluid Mech.*, **228**, 561.

Schuller, T., Durox, D., and Candel, S. (2003) A unified model for the prediction of laminar flame transfer functions: Comparisons between conical and V-flame dynamics. *Combust. Flame*, **134**, 21–34.

Subbaiah, M.V. (1983) Nonsteady flame spreading in two-dimensional ducts. *AIAA J.*, **21**, 1557–1564.

Ulitsky, M. and Collins, L.R. (1997) Relative importance of coherent structures vs. background turbulence in the propagation of a premixed flame. *Combust. Flame*, **111**, 257–275.

Wang, T.L. and Yang, V. (1997) Modeling of longitudinal combustion instability in a gas-turbine combustor. *AIAA Paper*, 1997–0694.

Williams, F.A. (1985) *Combustion Theory*, Benjamin/Cummins, Menlo Park, CA, pp. 411–415.

Yang, V. and Culick, F.E.C. (1986) Analysis of low frequency combustion instabilities in a laboratory ramjet combustor. *Combust. Sci. Technol.*, **45**, 1–25.

You, D. (2004) A Three Dimensional Linear Acoustic Analysis of Gas-Turbine Combustion Instability. Ph.D. Thesis, Department of Mechanical Engineering, Pennsylvania State University.

You, D., Sun, X., and Yang, V. (2003) A three-dimensional linear acoustic analysis of gas turbine combustion instability. *AIAA Paper*, 2003–0118.